Impact of structure and morphology on charge transport in semiconducting oligomeric thin-film devices

Melzer, C; Brinkmann, M; Krasnikov, VV; Hadziioannou, G

Published in:
Chemphyschem

DOI:
10.1002/cphc.200500142

Publication date:
2005

CHEMPHYSCHEM

DOI: 10.1002/cphc.200500142

Impact of Structure and Morphology on Charge Transport in Semiconducting Oligomeric Thin-Film Devices

Christian Melzer,[c] Martin Brinkmann,*[a] Victor V. Krasnikov,[d] and Georges Hadziioannou*[b]

*We investigated various thin-film morphologies of vacuum-deposited highly luminescent 2,5-di-*n*-octyloxy-1,4-bis[4′-(styryl)styryl]benzene (Ooct-OPV5) in a typical light-emitting-diode device structure. Important modifications in the thin-film morphology and structure were obtained by changing the substrate temperature in the range 23–90 °C. Structural analysis by X-ray and electron diffraction provided clear evidence for polymorphism in evaporated thin films of Ooct-OPV5. Concomitantly, the hole mobility in the corresponding devices was determined by transient electroluminescence measurements. We demonstrate that the substrate temperature T_{sub} is a key parameter that controls the hole mobility of the devices. Increasing T_{sub} between 23 and 84 °C results in a progressive increase of the zero-field hole mobility from 10^{-6} to 10^{-4} $cm^2 V^{-1} s^{-1}$. The increase in hole mobility is correlated to the average grain size in the thin films. In addition, we give evidence for the existence of a peculiar growth mode in the bulk crystal structure of Ooct-OPV5, whereby the (a,b) and (b,c) planes can grow in a homoepitaxial manner.*

1. Introduction

The semiconducting nature of materials based on conjugated organic molecules finds its origin in π-orbital overlap and the resulting delocalization of π electrons. While intramolecular charge transport in such molecules is usually regarded as fast due to the large ππ overlap along the molecule, charge transport through the bulk material is governed by π stacking of adjacent molecules. The semiconducting properties of the bulk material are therefore dependent on the mutual orientation and interchain distance of conjugated segments. Since in most of the conceivable and attractive applications based on organic semiconductors, such as field-effect transistors,[1] light-emitting diodes (LEDs),[2] and photovoltaic cells,[3] the device structure is planar, molecular long-range ordering with continuous π stacking along the preferential current direction is desirable. Moreover, grain boundaries in a polycrystalline system or disorder in an amorphous material are known to have tremendous impact on charge-carrier transport in the respective films.[4] Information about the molecular arrangement in thin films is therefore useful for assessing the suitability of a given organic conjugated material for semiconductor applications.

Due to excellent control over the chemical structure and their low molecular weight, conjugated oligomers exhibit the useful property of a high crystallinity,[5] which allows the preparation of high-purity polycrystalline thin films by thermal vacuum deposition techniques, and can occasionally result in the desired long-range order in the solid state. By controlling the deposition conditions, such as evaporation rate and substrate temperature, particular thin-film morphologies with distinct crystallite perfection, size, and orientation can be obtained. Here we report on the morphology and hole-transport properties of thin films based on highly crystalline 2,5-di-*n*-octyloxy-1,4-bis[4′-(styryl)styryl]benzene (Ooct-OPV5, Figure 1a). The single-crystal structure of' Ooct-OPV5 has been previously determined and is monoclinic, space group *I*2/*a*, $a = 36.2$, $b = 7.54$, $c = 36.6$ Å, $\beta = 116.85°$, $Z = 8$.[6] Additionally, thin-film morphologies of Ooct-OPV5 were earlier investigated,[6b,7] their impact on the optical properties of the films was unveiled,[6b] and results on the device performance of field-effect transistors (FETs)[1b] and light-emitting diodes (LEDs) employing thin films of this material were presented.[6b] In contrast to these previous studies, we focused on the determination of the thin-film morphology in an actual LED configuration, providing new results concerning the structure and morphology in thin films of Ooct-OPV5 and giving meaningful information about the relation between morphology and device performance.

[a] *Dr. M. Brinkmann*
Institut Charles Sadron, CNRS–UPR 22, 6, rue Boussingault BP 40016
67083 Strasbourg Cedex (France)
Fax: (+33) 388-414-099
E-mail: brinkmann@ics.u-strasbg.fr

[b] *Prof. Dr. G. Hadziioannou*
Laboratoire d'Ingénierie des Polymères pour les Hautes Technologies (LIPHT)
FRE 2711 CNRS, Ecole Européenne Chimie Polymères Matériaux (ECPM)
Université Louis Pasteur Strasbourg, 25, rue Becquerel
67087 Strasbourg Cedex 2 (France)
Fax: (+33) 390-242-716
E-mail: hadzii@ecpm.u-strasbg.fr

[c] *Dr. C. Melzer*
Institute of Materials Science, Darmstadt University of Technology
Petersenstrasse 23, 64287 Darmstadt (Germany)

[d] *Dr. V. V. Krasnikov*
Laboratory for Chemical Physics, Material Science Centre
University of Groningen, Nijenborgh 4
9747 AG Groningen (The Netherlands)

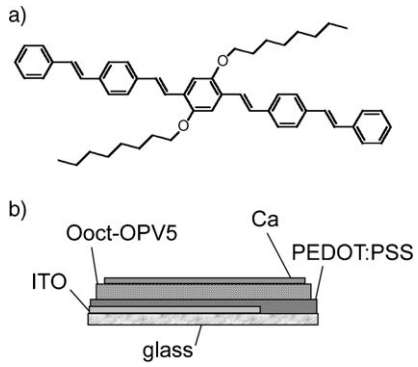

Figure 1. a) Chemical structure of Ooct-OPV5. b) Investigated device structure.

2. Results and Discussion

We prepared thin-film LEDs (Figure 1 b) by thermal vacuum deposition of Ooct-OPV5 on indium tin oxide (ITO)-coated glass substrate covered with a thin film of poly(3,4-ethylene dioxythiophene), PEDOT, highly doped with poly(styrenesulfonic acid), PSS. Calcium served as counterelectrode. While the deposition rate was kept constant for each thin-film deposition, the substrate temperature T_{sub} was varied in the range $23 \leq T_{sub} \leq 90\,^{\circ}C$.

2.1. Polymorphism

We used both XRD (in θ, 2θ mode) and electron diffraction (ED) to analyze the dependence of the thin-film structure on substrate temperature. XRD was first employed to identify the contact plane of Ooct-OPV5 crystallites on the PEDOT:PSS substrate.

The evolution of the XRD pattern with increasing T_{sub} is depicted in Figure 2, and the reticular distances d_{hkl} of the main diffraction peaks are summarized in Table 1. For all thin films, we observe two sets of diffraction peaks centered around $2\theta = 6.0^{\circ}$ and $2\theta = 5.3^{\circ}$, as well as the corresponding second-order peaks around $2\theta = 12^{\circ}$. The first set of peaks around $2\theta = 6.0^{\circ}$ involves two peaks with d_{hkl} values of 15.5–15.6 Å and 15.15–15.2 Å, except for $T_{sub} = 23\,^{\circ}C$, where the peaks are merged because of the small grain size, as determined from AFM measurements (see below). For $T_{sub} = 54\,^{\circ}C$ we also observe the second order of these peaks for $d_{hkl} = 7.64$ and 7.44 Å. For $T_{sub} \geq 54\,^{\circ}C$ we observe two additional peaks at 16.90 and 16.40 Å whose intensity also increases with increasing T_{sub}. Overall, the increase of T_{sub} results in both an important increase of the peak intensity and a narrowing of the peak width. All these observations are clear indications for the increased crystallinity of the films at higher T_{sub}. In addition, the evolution of the X-ray diffractogram also suggests either a change of preferential orientation of the crystalline domains or a change of crystal structure, that is, polymorphism with increasing T_{sub}.

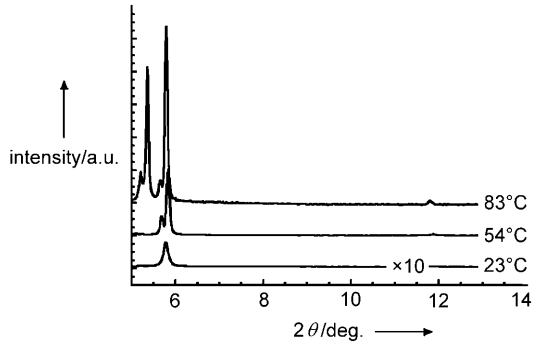

Figure 2. Evolution of the X-ray diffractogram of Ooct-OPV5 thin films vacuum-deposited on ITO/PEDOT:PSS substrates with increasing substrate temperature T_{sub}.

Table 1. d_{hkl} reticular distances observed by XRD (θ, 2θ) ($\lambda = 1.540$ Å) in Ooct-OPV5 thin films deposited on ITO/PEODT:PSS substrates at different T_{sub}.

	α-phase d_{hkl} [Å]		β-phase d_{hkl} [Å]	
T_{sub} [°C]	(002)	(200)	(002)	(200)
23	15.28		17.0	
54	15.50	15.15	17.1	16.7
83	15.60	15.22	16.9	16.4

Let us now try to identify the origin of the two sets of diffraction peaks observed for $2\theta \leq 7^{\circ}$. Considering the known single-crystal structure of Ooct-OPV5 at $T = 130$ K,[6] the 16.90 and 16.40 Å reflections of the XRD diffractograms are close to the calculated values of 16.34 Å and 16.15 Å for the (002) and (200) reflections, respectively. The difference between calculated and observed d_{hkl} values is ascribed to the expansion of the unit cell between 130 K and room temperature. From the known bulk crystal structure, the calculated relative intensities of the (002) and (200) reflections amount to 100 and 3.7 %, respectively. However, in Figure 2, we observe that the (200) peak shows the strongest intensity. Hence, we deduce that the (200) orientation of the microcrystallites corresponds to the dominant contact plane. The two contact planes are depicted in Figure 3 a, and the predicted equilibrium morphology of the microcrystallites in Figure 3 b.[1] As can be seen in Figure 3 a, the (200) contact plane involves the conjugated phenyl ring of the Ooct-OPV5 molecules, which have their long axis inclined at 44° with respect to the normal of the plane. In contrast, the (002) contact plane involves the aliphatic chains, and the long molecular axis is inclined at 71° with respect to the normal to the plane.

In contrast to the 16.90 and 16.40 Å reflections, both the 15.50 and 15.15 Å reflections observed at low T_{sub} cannot be in-

[1] *The growth morphology of the crystal was obtained by using the Hartmann and Perdock formalism. The crystal shape is determined by the growth rates of the crystal faces, which are proportional to the attachment energies* E_{hkl} *of the slices (*hkl*). E_{hkl} corresponds to the energy release per structural unit as a crystal slice (*hkl*) attaches to the crystal surface from an infinite distance. Only van der Waals interactions are taken into account in this calculation. For further information, see the Cerius Users Guide section on Computational & Analytical Instrumentation, pp. 131–143 and references therein.*

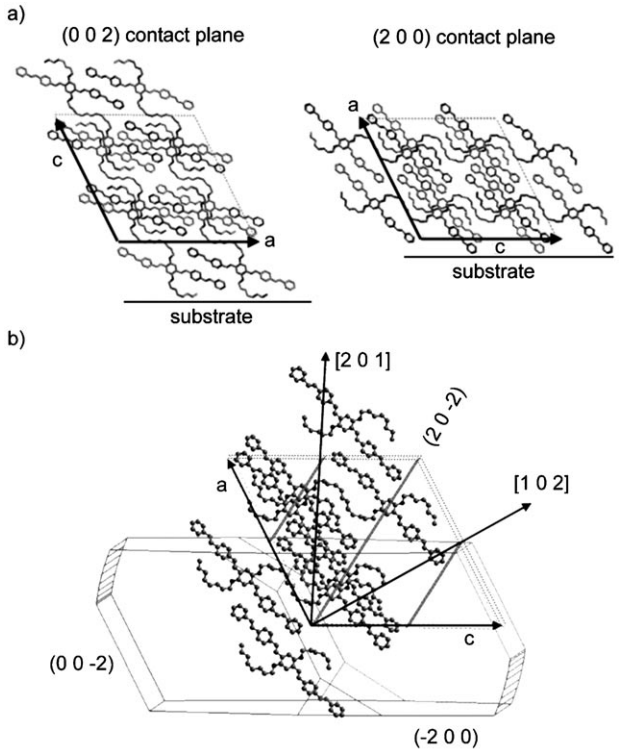

Figure 3. a) Molecular models showing the two orientations of the unit cell with respect to the substrate (contact planes). b) Growth morphology of an Ooct-OPV5 crystal and relative orientation of the unit cell as well as orientations of the zone axes.

dexed on the basis of the structure of the bulk polymorph. Indeed, from the known crystal structure refined at 130 K, only one single reflection at 15.51 Å and corresponding to the (20$\underline{2}$) plane is expected and not a doublet as observed in our case. In addition, if we take into account the typical expansion coefficient of the unit cell of a molecular crystal (ca. 0.001 Å K^{-1} [8]) between 130 K and room temperature, we would expect the (20$\underline{2}$) reflection to appear at a d_{hkl} value of 15.7–15.8 Å, which is significantly larger than the observed values of 15.50 and 15.15 Å. We therefore propose that the 15.50 and the 15.15 Å reflections originate from a low-temperature polymorph (hereafter α-phase), of which the structure is not known yet. Assuming rather similar crystal packings for the α and the β polymorphs, we can infer that the two structures mainly differ in either the compactness of the aliphatic chain layer or the inclination of the principal molecular axis of OoctOPV5 in the unit cell, which is commonly observed in conjugated molecular crystals.[8]

In summary, the 16.90 Å and 16.40 Å reflections belong to a high-temperature polymorph (β-phase), of which the structure is the same as the known single-crystal structure (see below). The β structure is the dominant crystal structure at $T_{sub} \geq 90\,^{\circ}C$, whereas at low substrate temperatures ($T_{sub} \leq 90\,^{\circ}C$) a different polymorph (α) characterized by the 15.50 and 15.15 Å reflections is observed to be the dominant crystal form. Note that both α and β structures coexist in variable proportions over a rather broad T_{sub} range of $54\,^{\circ}C \leq T_{sub} \leq 90\,^{\circ}C$. This coexistence of polymorphs can also be considered as an important origin of structural disorder in the films, which affects charge transport in the device.

2.2. Device Morphology

The deposition of Ooct-OPV5 on an ITO/PEDOT:PSS substrate at $T_{sub} = 23\,^{\circ}C$ resulted in a rough granular structure that indicates the presence of some extended crystallites. The observation of birefringence by cross-polarized microscopy supports this interpretation (Figure 4). Tapping-mode AFM revealed domains of wedgelike shape with a typical size of $0.05 \times 0.4\ \mu m^2$ (Figure 5). A thin-film RMS roughness of 8 nm was found. The

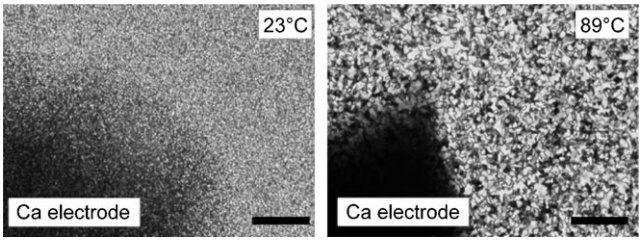

Figure 4. Polarized-light optical micrographs of Ooct-OPV5 thin-film devices obtained at different T_{sub} on ITO/PEDOT:PSS substrates. Scale bar: 50 μm.

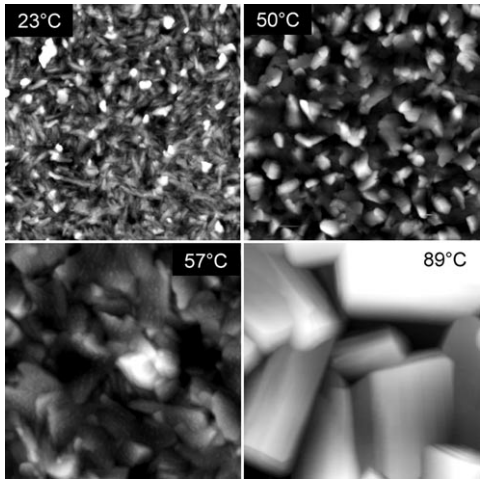

Figure 5. Topographical map ($4 \times 4\ \mu m^2$) of Ooct-OPV5 thin films deposited at different substrate temperatures T_{sub}, obtained by tapping-mode AFM. The maximal heights of the topographical maps are 50, 90, 190, and 340 nm for $T_{sub} = 23$, 50, 57, and 89 °C, respectively.

domains of equal molecular orientation, which resulted in areas of equal light intensity in cross-polarized microscopy, were several micrometers in size, that is, much larger than the domains observed by AFM. This clearly evidences the existence of correlations in the orientation of adjacent Ooct-OPV5 domains. This is moreover supported by the electron diffraction (ED) patterns (Figure 6), which show the presence of arcing (see below). Increasing T_{sub} during Ooct-OPV5 deposition results in an increase of the mean size of crystalline domains. The transition in morphology was most pronounced in the

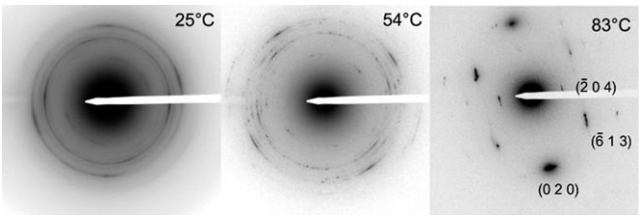

Figure 6. Electron diffraction (ED) pattern of Ooct-OPV5 thin films deposited at different T_{sub} on an ITO/PEDOT:PSS substrate.

range of 50–60 °C, which is in agreement with earlier findings.[9] The RMS roughness ($4\times4\ \mu m^2$ area) and the mean domain size obtained by AFM are listed in Table 2. Increasing

Table 2. RMS roughness and domain size of thin films of Ooct-OPV5 at different T_{sub} obtained by tapping-mode AFM.

T_{sub} [°C]	23	50	57	89
Domain size [μm^2]	0.02	0.07	0.2	3
RMS roughness [nm] ($4\times4\ \mu m^2$)	8	13	23	60

T_{sub} also results in a change of the microcrystallite shape from wedgelike at $T_{sub}=23$ °C to extended platelets for $T_{sub}\geq60$ °C, with in-plane dimensions exceeding the nominal film thickness, and hence strongly reduced number of grain boundaries that must be crossed by charge carriers. The increase in crystallinity in Ooct-PV5 films deposited at $T_{sub}\geq60$ °C has also been evidenced by XRD (see below) and results in a significant increase of RMS film roughness from 8 nm at $T_{sub}=23$ °C to 60 nm at $T_{sub}=89$ °C ($4\times4\ \mu m^2$). This roughness affects the Ca/Ooct-OPV5 interface. The topography of the Ca layer exhibits a granular texture with an average grain size in the range 10–50 nm, whereby the Ca grains decorate gently the organic thin film. The important point is that the roughness of the Ca/Ooct-OPV5 interface stems mainly from the underlying organic layer and not from the evaporated Ca electrode.

2.3. Transient Electroluminescence Measurements

The above structural and morphological study of the devices evidenced both a change in crystal structure (α vs β form) and an increase in average grain size with increasing T_{sub}. We studied how these modifications influence the corresponding transport properties in the OLED devices.

To determine the hole mobility in the respective Ooct-OPV5 films, we used transient electroluminescence (EL) measurements, which is a well-established method to estimate the charge-carrier mobility in highly luminescent organic thin films.[10] In transient EL an abrupt electrical stimulus drives electron and hole charge-carrier fronts oppositely through an LED, until they meet and radiative recombination occurs. The appearance of the EL signal is delayed with respect to the stimulus, and the delay time is determined by both the hole and the electron transit times.

A detailed analysis of nondispersive EL transients obtained from materials like poly(phenylene vinylene), PPV, was elaborated by Pinner et al.[10b]. In agreement with their observations, the delayed EL signal obtained from Ooct-OPV5-based LEDs increased double-exponentially. According to Pinner et al., the transit time τ_h for the faster charge carrier species—typically holes in PPV-type materials—is then given by t_d+t_1, where t_d is the initial delay time after which the first recombination occurs, and t_1 is the time after which the charge distribution of the faster charge-carriers is fully established. An increase in EL after t_d+t_1 is due to buildup of the charge-carrier distribution of the slower electrons. From the unveiled τ_h, we determined the hole mobility μ_h with $\mu_h=d/(\tau_h F)$, where d is the thickness of the semiconductor layer and F the electric field.

The resulting hole mobilities for a variety of Ooct-OPV5 thin films as a function of the square root of the field can be seen in Figure 7. The μ_h obtained from Ooct-OPV5 thin-film LEDs prepared at room temperature is field-activated according to a Pool–Frenkel-like equation [Eq. (1)]:[11]

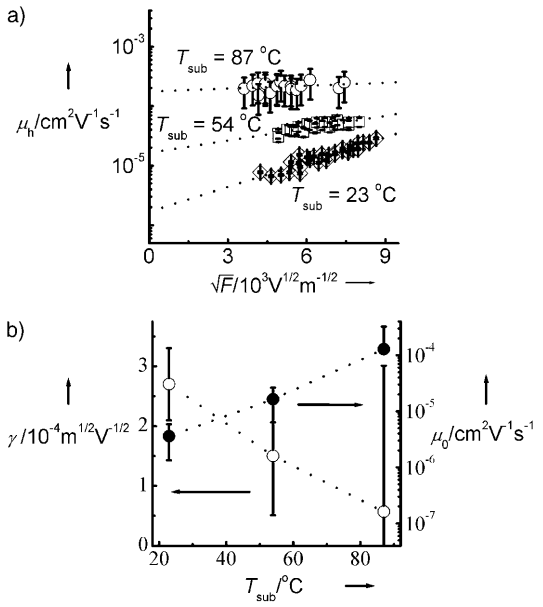

Figure 7. a) Hole mobility of Ooct-OPV5 measured in thin films that were deposited at different T_{sub}. The error bars indicate the error due to roughness of the thin film. b) Field-activation factor γ (○) and zero-field hole mobility μ_0 (●) of Ooct-OPV5 for different T_{sub}.

$$\mu_h=\mu_0\cdot\exp\left[\gamma\sqrt{F}\right] \quad (1)$$

with a field activation factor γ of $2.7\times10^{-4}\ m^{1/2}V^{-1/2}$ and a zero-field hole mobility μ_0 of $3.6\times10^{-6}\ cm^2V^{-1}s^{-1}$. This is in accordance with μ_h found by Geens et al., employing field-effect measurements.[1b] For thin films deposited at elevated T_{sub}, γ strongly decreased, while μ_0 increased. However, due to the pronounced roughness of Ooct-OPV5 thin films (see Figure 5), especially when deposited at elevated T_{sub} (typically $T_{sub}\geq60$ °C), our measurements on a planar device structure might be affected by fluctuations in the thickness of the active layer.

Especially the transit distances of carriers and the electric field distribution in the device are likely to be influenced by the morphology of the organic semiconducting layer. For devices prepared at high T_{sub}, we found an increased probability of finding shorted devices. Nonetheless, the trend in the evolution of μ_h with T_{sub} is significant and sizeable. Figure 7 plots the relation between μ_0 and γ, respectively, and T_{sub}.

From Table 2 and Figure 7, it is apparent that the increase in hole mobility with increasing T_{sub} coincides with an increase in the average domain size: the larger the average domain size, the higher the zero-field mobility μ_0 and the lower the field dependence of the hole mobility. A similar observation has been reported for polycrystalline oligothiophene thin films: The field-effect mobility measured in planar field effect transistors (FETs) increases (and becomes less temperature-dependent) with increasing mean domain size.[4a] Note that the increase in hole mobility with increasing T_{sub} coincides with the emergence of the bulk crystal structure in the thin films. This last point may also suggest a larger hole mobility in the β than in the α polymorph because of more favorable π stacking in the β polymorph.

In general, the carrier mobility in a polycrystalline film is given by Equation (2):

$$(d_g + d_b)/\mu = d_g/\mu_g + d_b/\mu_b \quad (2)$$

where μ_b and μ_g are the mobilities, and d_b and d_g the dimensions of a grain boundary and the grains, respectively. Presumably, more defect states are located in the grain boundary than in the grain, and $\mu_g > \mu_b$ holds. Consequently, from Equation (2), the mobility increases with increasing crystallite size. Moreover, Horowitz et al. pointed out that due to the defect states in the grain boundary a back-to-back Schottky barrier emerges at the grain boundaries.[4a] If the grain size is longer than the Debye length, the Schottky barrier at the grain boundaries is important, and the transport across the grain boundary is described by the thermionic emission rate. On the other hand, if the grain size becomes much smaller than the Debye length, the system is described by a uniform distribution of localized states throughout the semiconductor. From the back-to-back Schottky barrier picture it can be shown that in the former case the effective mobility increases linearly with the mean domain size.

2.4. Electron Diffraction and Evidence for Homoepitaxy in the β Polymorph

A typical evolution of the ED pattern as a function of T_{sub} is depicted in Figure 6. In accordance with the AFM results, the ED pattern of the films grown at $T_{sub} = 23\,^{\circ}C$ shows nonuniform azimuthal intensities, which indicate that the in-plane orientations of the adjacent Ooct-OPV5 domains observed by AFM are correlated over areas of several micrometers in size. This result is in agreement with the observations made by polarized optical microscopy (see above). With increasing T_{sub}, the ED reflections become sharper and narrower, which is consistent with the increase in domain size observed by AFM. The most intense reflections for $T_{sub} = 23$ and $54\,^{\circ}C$ correspond to reticular distances of 4.73 and 3.96 Å. The latter d_{hkl} value is close to the π-stacking distance in the β polymorph, that is, 3.86 Å. Hence, we may infer that the 4.73 Å distance corresponds to the π-stacking distance in the α polymorph. However, both these π-stacking distances are significantly larger than the typical values found in conjugated systems, which lie usually in the range 3.3–3.4 Å,[12] that is, even in the π-stacking direction (*b* axis) no strong orbital overlaps exist. Hence, it is expected that the charge-carrier transport is of the hopping type.

For $T_{sub} = 89\,^{\circ}C$, we obtained the ED pattern of single β domains of a few micrometers in size by using selected-area electron diffraction (SAED). For comparison, we also observed the ED pattern of a single crystallite obtained by fast cooling from a saturated THF/methanol solution (see ref. [6b]). The similarity of the SAED and ED patterns of the single-crystalline sample supports the previous identification of the β form by XRD as the high-T_{sub} polymorph.

To identify the crystal orientation in the thin films, we simulated the ED pattern using the Cerius software package. In agreement with the computer-simulated ED patterns, the most intense reflection is indexed as 020 with $d_{020} = 3.86$ Å. Consequently, and in agreement with the XRD data, the "π-stacking-axis" lies in the plane of the substrate.

Figure 8 depicts the calculated ED patterns corresponding to the (002) and the (200) contact planes, which correspond to the [102] and [201] zone axes, respectively. The orientations of the zone axes with respect to the crystal are shown in Figure 3b. If we consider a (002) orientation of the crystal, we can account for all the reflections in the ED pattern of Figure 6 except for the reflection corresponding to a d_{hkl} of 9.1 Å. The same observation can be made on the ED pattern of a β single crystal of Ooct-OPV5 grown from THF/methanol solution.[6b] Using the known β structure of Ooct-OPV5, the reflection corresponding to $d_{hkl} = 9.1$ Å can be indexed as (20$\underline{4}$) and is perfectly accounted for if we consider a crystal with (200) orientation, that is, a [201] zone axis. Since the (20$\underline{4}$) reflection is also observed in the ED pattern of the single crystal domain, as shown in Figure 6, we assume that the ED pattern corresponds to the overlap of two distinct patterns corresponding to (200) and (002) orientations with identical *b* axis orientation. Hence, we infer that domains with both (200) and (002) orientations coexist in single-crystalline domains of the β form of Ooct-OPV5. This explanation is in perfect agreement with the XRD data (see above).

The coexistence of [102] and [201] orientations for the same β crystal can be explained by a mechanism of homoepitaxial growth of the (100) face on the (001) face and vice versa. Indeed, the (*ab*) and (*bc*) planes of the β polymorph share almost the same unit-cell parameters, since *a* and *c* are almost equal ($a = 36.2$ Å vs $c = 36.6$ Å). Considering the bulk crystal structure of Ooct-OPV5, a 180° rotation of the unit cell axis along the [101] twin axis exchanges the (*ab*) and (*bc*) planes. Such a twinning mechanism is known to induce fine structures, for example, streaking in the ED pattern, as is observed for the (20$\underline{4}$) and (61$\underline{3}$) reflections (see Figure 6).[13] The streaking is typically caused by strain at a twin interface, and the strain is

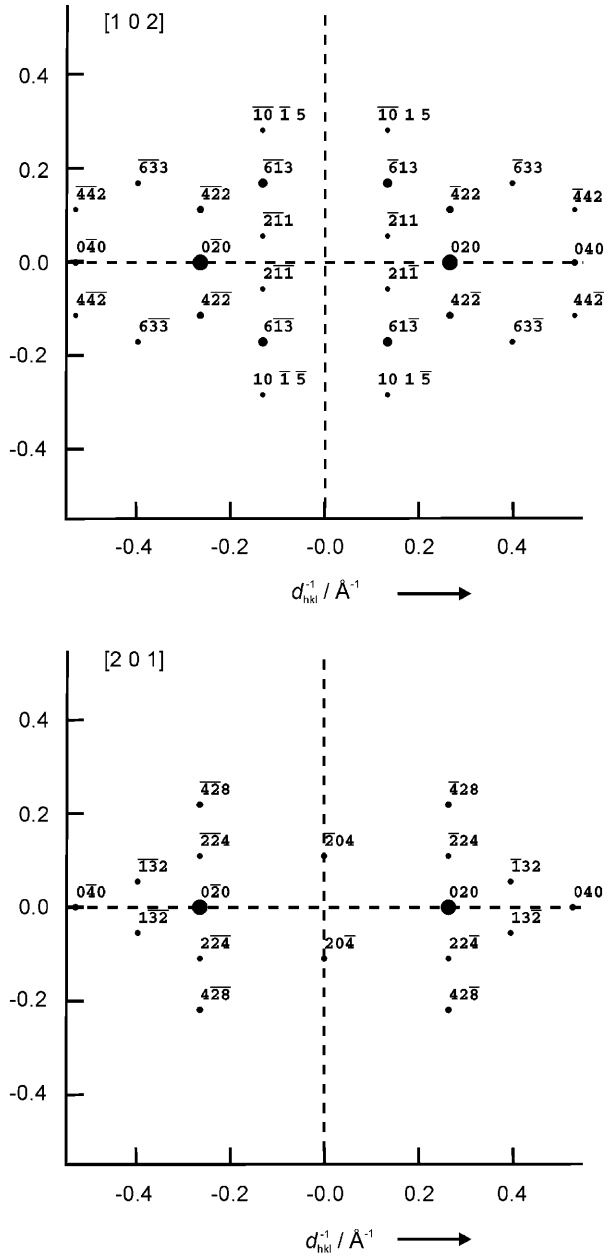

Figure 8. Calculated ED patterns for two different zone axes of a single crystal of Ooct-OPV5 by using the bulk crystal structure refined at 130 K.

due to the lattice mismatch between *a* and *c* parameters ($\Delta = (c-a)/c \approx 1\,\%$). We can anticipate that the presence of strain at the twin interface directly translates into charge carrier traps or scatter centers. However, if we model the interface between (*ab*) and (*bc*) planes as shown in Figure 9, matching of the positions of the terminal phenyl groups of the Ooct-OPV5 molecule in the (*bc*) plane with the corresponding phenyl groups in the (*ab*) plane is observed. Possibly, improved $\pi\pi$ interaction between the terminal phenyl rings at the interface between the (*ab*) and (*bc*) planes favors the homoepitaxy phenomenon and additionally assists charge transfer across the twining interface.

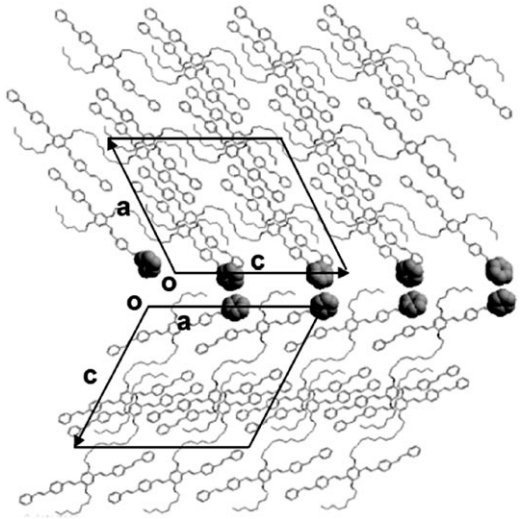

Figure 9. Molecular model of the interface between the (*ab*) and (*bc*) planes growing in a homoepitaxial manner. The terminal phenyl groups at the interface are drawn as balls to highlight the matching of cell parameters at the interface.

3. Conclusions

The thin-film morphology of vacuum-deposited Ooct-OPV5 on a typical anode of ITO/PEDOT:PPS at different substrate temperatures was investigated. In general, Ooct-OPV5 thin films consisted of two polymorphs. The α-phase is predominant when films are deposited at low T_{sub} ($T_{sub} \leq 90\,^{\circ}C$), whereas the β-phase is more abundant for $T_{sub} \geq 90\,^{\circ}C$. The structure of the high-temperature polymorph (β-phase) coincides with the known single crystal structure of Ooct-OPV5, while that of the low-temperature polymorph corresponds to a new polymorph. Even though the impact of the occurrence of the two polymorphs on the hole transport properties could not be clearly identified, their coexistence is expected to introduce additional sources for structural disorder in the thin films. A clear trend has been observed between the hole mobility and the film morphology in terms of changes in crystal size, involving a reduction of grain boundaries for films prepared at elevated T_{sub} (above 60 °C). This evolution of the organic semiconductor properties results in a considerably improved hole mobility for polycrystalline films with larger crystalline domains.

Experimental Section

Thin films of Ooct-OPV5 were deposited on a typical anode used in the field of photovoltaic cells and LEDs, namely, an ITO-coated glass substrate covered with a thin film of PEDOT highly doped with PSS.[14] Prepatterned ITO-coated glass substrates were wet-cleaned, and thin layers (ca. 80 nm) of PEDOT:PSS (Bytron P TP AI 4083) were deposited by spin-coating from a water dispersion. The layers were dried under high vacuum at elevated temperature. Subsequently, thin films of Ooct-OPV5 (200–250 nm thickness) were thermally vacuum-deposited at 10^{-7} mbar. While the deposition rate was kept constant at a rate of 0.5 Å s^{-1} for each thin-film deposition, the substrate temperature T_{sub} was varied from 23 to

90 °C. Next, calcium counterelectrodes were deposited at 10^{-6} mbar on top of the organic semiconductor layer.

The hole-transport properties of the respective Ooct-OPV5 films were determined by transient electroluminescence (EL) measurements in a nitrogen atmosphere.[10] A planar LED was exposed to a short voltage pulse (typically larger than 10 μs) in forward bias direction, and the light emitted upon this stimulus was collected by a photodetector.

The morphologies of the resulting polycrystalline films in the LED structure were investigated by optical microscopy, [XRD (θ, 2θ)], AFM in tapping mode (Nanoscope III equipped with Si tips (25–50 N m^{-1} and 280–360 kHz)), and TEM. XRD measurements were performed on a Siemens D5000 spectrometer with $Cu_{K\alpha}$ radiation ($\lambda = 1.540$ Å). TEM samples were prepared by depositing a thin carbon film on the Ooct-OPV5 sample. Polyacrylic acid droplets were deposited on the film and left to dry. Subsequently, the polyacrylic lentils were stripped off from the substrate and floated on water. Then, the carbon/Ooct-OPV5 bilayers were deposited onto copper grids. The electron diffraction patterns were obtained with a CM12 microscope equipped with a MVIII CCD camera.

Acknowledgments

Christian Chaumont is gratefully acknowledged for his help in X-ray diffraction analysis. T. Heiser, B. Lotz, and J.-C. Wittmann are gratefully acknowledged for stimulating discussions.

Keywords: charge-carrier transport · conducting materials · crystal growth · polymorphism · thin films

[1] a) F. Garnier, G. Horowitz, G. Peng, D. Fichou, *Adv. Mater.* **1990**, *2*, 592–594; b) W. Geens, D. Tsamouras, J. Poortmans, G. Hadziioannou, *Synth. Met.* **2001**, *122*, 191–194.

[2] a) C. Adachi, A. Tsutsui, S. Saito, *Appl. Phys. Lett.* **1990**, *56*, 799–801; b) J. Kalinowski, *J. Phys. D* **1999**, *32*, R179-R250.

[3] a) S. E. Shaheen, C. J. Brabec, N. S. Sariciftci, F. Padinger, T. Fromherz, J. C. Hummelen, *Appl. Phys. Lett.* **2001**, *78*, 841–843; b) C. Melzer, V. V. Krasnikov, G. Hadziioannou, *Appl. Phys. Lett.* **2003**, *82*, 3101–3103.

[4] a) G. Horowitz, M. E. Hajlaoui, *Adv. Mater.* **2000**, *12*, 1046–1050; b) H. Bässler, *Phys. Status Solidi B* **1993**, *175*, 15–56.

[5] H. E. Katz, S. F. Bent, W. F. Wilson, M. L. Schilling, S. B. Ungashe, *J. Am. Chem. Soc.* **1994**, *116*, 6631–6635.

[6] a) R. E. Gill, A. Meetsma, G. Hadziioannou, *Adv. Mater.* **1996**, *8*, 212–214; b) R. E. Gill, *PhD Thesis*, Rijksuniversiteit Groningen,The Netherlands, **1996**.

[7] a) D. Tsamouras, G. Palasantzas, J. T. M. De Hosson, *Appl. Phys. Lett.* **2001**, *79*, 1801–1803; b) G. Palasantzas, D. Tsamouras, J. T. M. De Hosson, *Surf. Sci.* **2002**, *507–510*, 357–361.

[8] A. I. Kitaigorodsky, *Molecular Crystals and Molecules*, Academic Press, New York, **1973**, p. 294.

[9] D. Tsamouras, G. Palasantzas, *Appl. Phys. Lett.* **2002**, *80*, 4528–4530.

[10] a) P. W. M. Blom, M. C. J. M. Vissenberg, *Phys. Rev. Lett.* **1998**, *80*, 3819–3822; b) D. J. Pinner, R. H. Friend, N. Tessler, *J. Appl. Phys.* **1999**, *86*, 5116–5130; c) T. C. Wong, J. Kovac, C. S. Lee, L. S. Hung, S. T. Lee, *Chem. Phys. Lett.* **2001**, *334*, 61–64; d) J. Wang, R. G. Sun, G. Yu, A. J. Heeger, *J. Appl. Phys.* **2002**, *91*, 2417–2422.

[11] P. M. Borsenberger, D. S. Weiss, *Organic Photoreceptors for Imaging Systems*, Marcel Dekker, New York, **1993**, p. 154.

[12] M. S. Dresselhaus, G. Dresselhaus, *Adv. Phys.* **1981**, *30*, 139–326.

[13] P. B. Hirsch, *Electron Microscopy of Thin Crystals*, Butterworth, London, **1965**, p. 141.

[14] a) A. C. Arias, M. Granström, D. S. Thomas, K. Petritsch, R. H. Friend, *Phys. Rev. B* **1999**, *60*, 1854–1860; b) L. B. Groenendaal, F. Jonas, D. Freitag, H. Pielartzik, J. R. Reynolds, *Adv. Mater.* **2000**, *12*, 481–494.

Received: March 14, 2005
Revised: June 20, 2005
Published online on October 11, 2005

